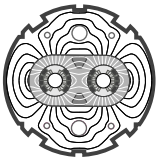

LHC Project Note 208

5 October 1999

Bernard.Jeanneret@cern.ch

Beam losses far downstream of the high luminosity interaction points of LHC - intermediate results

I. Baishev*, J.B. Jeanneret and G.R. Stevenson

Keywords: interaction, dispersion, beam loss, collimator

Summary

We report a study on beam losses in the insertions IR1 and IR5 of LHC. We considered proton-proton collisions with a relatively small momentum transfer which induce distant losses. We show that the level of these losses is high enough to quench the quadrupoles Q5 in the straight sections and probably the dipoles B8 in the dispersion suppressors. We confirm that collimators upstream of Q5 can prevent those quenches. Beam loss distributions in the dispersion suppressors are computed in the presence of these collimators and associated radiological results are discussed. Associated cryogenic power load are quantified.

1 Introduction

The products of proton-proton collisions in LHC are basically of three kinds. Most of these particles have a low momentum and a large emission angle compared to the beam. In IP1 and IP5 most of them will be captured by the TAS and TAN absorbers. Elastically scattered protons have small angular and momentum deviations and stay inside the acceptance of the ring. In between these two cases, inelastic diffractive losses can induce significant losses in the straight section and the dispersion suppressor adjacent to IP1 and IP5. In Section 2 we describe quantitatively this class of interactions. In an earlier study [1], only one species of diffractive interactions was considered. It described correctly the proton losses in the high dispersion part of the dispersion suppressor, but underestimated the losses upstream of that area. We show in Section 4 that if no additional protection is added, the quadrupole Q5 and most likely the dipoles B8 would quench. We therefore propose to install a collimator in the warm section located in front of Q5 to solve this problem. We then build a map of losses between Q7 and Q17 (Section 5.2) and finally some radiological elements are discussed for

*Institute for High Energy Physics, Protvino, Russia.
Member of the Russian collaboration to the LHC Project.

these areas.

We lately included the beam-beam crossing bumps to our tracking work, together with the newly proposed beam screens in some insertion magnets. The results indicate that the level of losses in D2 and Q4 is also near or above the quenchs limit. These levels are dependent on the orientation of the crossing plane. A more detailed variational study is therefore necessary before an adequate local collimation scheme can be proposed. This will be presented in a separate document. These new facts do not affect the conclusions drawn here about the dispersion suppressors.

2 Basic parameters

The transverse excursion Δx_p caused by the difference between the proton momentum p and the central momentum of the beam p_0 is proportional to the dispersion D

$$\Delta x_p = \ D \cdot \delta_p \ , \tag{1}$$

where $\delta_p = \left|\frac{\delta p}{p_0}\right| = 1 - \frac{p}{p_0}$ is the relative momentum offset. In the particular case of a particle which suffers a localised momentum loss, the periodic dispersion shall be replaced by the dispersive contributions of traversed elements downstream of the point of the momentum loss. This is inherently treated by our step-tracking code (see Section3.3), in which momentum-dependent transfer matrices are built before a tracking step is made. Some dispersion is created in the straight section by the dogleg dipoles D1 and D2. It is relatively small but high enough to cause loss of proton with relatively high δ_p. The first noticeable aperture limitation downstream of the IP occurs at the TAN absorber. The maximum of the horizontal dispersion is reached in the arcs. Therefore we consider protons with $\delta_{p,min} < \delta p < \delta_{p,max}$ as candidates to be lost downstream of TAN but not further than in one of the first adjacent arc cells. With the horizontal half-aperture $r = \ 26$ mm and horizontal internal dispersion $D_x \approx 100$ mm at the TAN we get $\delta_{p,max} \approx 0.3$. In the arcs $D_{max} = 2.2$ m , $r = 22$ mm, then $\delta_{p,min} = 0.01$. The protons with $\delta_{p,min} < 0.01$ are the candidates for an interception by the momentum cleaning system in IR3.

3 Beam loss simulation

3.1 Proton-proton interactions

The kinematic variables s, q^2, x_F are used below for the presentation of the differential cross section for the inclusive reaction $p + p \rightarrow p + X$ in which X represents all possible final state of fragmentation of one of the colliding protons. The proton in the final state suffers a slight transverse kick and a momentum offset which is has a wide distribution which also strongly peaks near the nominal beam momentum. The variable s is the center of mass energy squared, x_F is the Feynman variable and $q^2 = -t$ is the 4-momentum transfer. At the LHC energies $x_F \approx 1 - \delta_p$ for small δ_p.

The differential cross section of single-diffraction (SD) is usually described by the PPP and PPR terms of the triple-Regge expansion (A 'P' means a Pomeron particle and 'R' a

Regge trajectory. Moreover the Regge-expansion is often used for phenomenological models of both SD and non-diffractive (ND) inclusive cross sections.

We choose the parametrisation of the PPP and PPR terms of [2]

$$\left(\frac{d^3\sigma}{dq^2dx_F}\right)_{PPP} = \left(2.32e^{-3.94q^2} + 0.33e^{-1.12q^2}\right)(1-x_F)^{0.72q^2-1} \tag{2}$$

$$\left(\frac{d^3\sigma}{dq^2dx_F}\right)_{PPR} = \frac{1}{\sqrt{S}}\left(0.95e^{0.01q^2} + 3.47e^{-4.41q^2}\right)(1-x_F)^{0.72q^2-1.5} \tag{3}$$

for a good description of the cross section at $x_F > 0.95$. To extend the description down to $x_F = 0.7$ we add the $\pi\pi P$ and RRP terms from [3]

$$\left(\frac{d^3\sigma}{dq^2dx_F}\right)_{\pi\pi P} = 19\pi q^2 \frac{(1-x_F)^{1+0.6q^2}}{\left(m_\pi^2+q^2\right)^2} e^{-4.3q^2} \tag{4}$$

$$\left(\frac{d^3\sigma}{dq^2dx_F}\right)_{RRP} = 3.3\pi(1-x_F)^{1.5q^2}e^{0.38q^2} \ . \tag{5}$$

Integrated over q^2, the differential cross sections $d\sigma/dx_F$ are shown in Figure (1). The importance of the non-diffractive component, which was ignored in [1], is clearly visible above $\delta_p > 0.01$. The integral σ^M of $d\sigma/dx_F$ between x_F=0.7 and x_F=0.99 is equal to 12.3 mbarn.

3.2 Rates

The differential rates are obtained with the relation

$$\frac{d^3N}{dq^2dx_F} \ = \ \mathcal{L} \ \cdot \ \frac{d^3\sigma}{dq^2dx_F} \ . \tag{6}$$

Our calculations are made with the nominal luminosity of LHC $\mathcal{L} = 10^{34}$ cm^{-2}s^{-1}.

3.3 Tracking

The STRUCT code [4] is used to track the proton scattered. The version 6.-2 of the optics is used to define the lattice of IR1/IR5 and their adjacent arc cells. The lattice elements are subdivided by ∼1 meter pieces for an accurate presentation of the beam loss density. The apertures are extracted from the database of geometrical aperture for LHC (see [5]).

4 A collimator near Q5

A first calculation of beam losses is done with the basic lattice and without any collimators in the straight section (see the dashed histogram in Figure 2). The largest loss rate of $4.2 \cdot 10^7$ protons s^{-1} occurs at the transition of 100 mm beam pipe to 50 mm beam pipe in front of the quadrupole Q5 (∼190 m downstream of IP). This loss rate is five times larger than the steady quench limit $\dot{n}_q = 8 \cdot 10^6$ protons m^{-1}s^{-1} [6] (considering an effective shower length $L_{shower} \simeq 1$ m [7]). Moreover the second peak of the loss density, which is

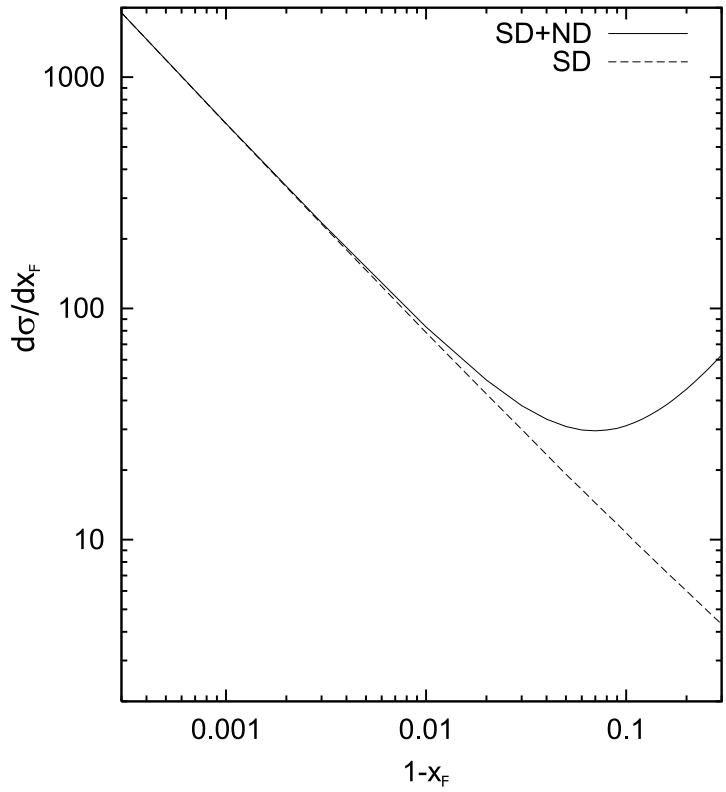

Figure 1: The differential cross-section $d\sigma/dx_F$ for single-diffractive (SD) and non-diffractive (ND) reactions as a function of $1 - x_F \simeq \delta_p$ at $\sqrt{s} = 14$ TeV.

located inside the dipole B8B (∼290 m downstream IP) and amounts to $4.4 \cdot 10^6$ m^{-1}s^{-1}, is dangerously close to the quench level.

Following [1], we introduce a horizontal collimator upstream of Q5 to protect both Q5 and B8B from quenching. Any location between Q4 and Q5 could be used because the horizontal dispersion is practically constant in this section. But in practice only the small warm section between the TOTEM detectors and the cryobox is available in IR5. In IR1 collimator can be placed closer to the exit of Q4. It can be a standard secondary collimator unit designed for the cleaning systems equipped with 50 cm copper jaws.

A second tracking session is made with this collimator installed. It should be noted that we do not treat the collimator as a 'black absorber'. We simulate scattering of protons in the collimator jaw following [8] so that the outscattered protons contribute to the beam losses downstream. The horizontal position of the jaw x_c can be chosen at $x_c \geq 10\sigma_x$ where σ_x is the horizontal r.m.s. size of the circulating beam. In this case the collimator will not interfere with the main beam cleaning section.

The beam loss density for the case $x_c = 15\sigma_x$ is given by the solid histogram in Figure 2. The loss rate at the beam pipe transition upstream of Q5 is 25 times lower than in the case without the collimator. However a full evaluation of the protection of Q5 quenching requires to take into account the energy deposition in Q5 coils associated to the secondary radiation produced in the collimator. Another study with cascade simulation in the collimator jaw

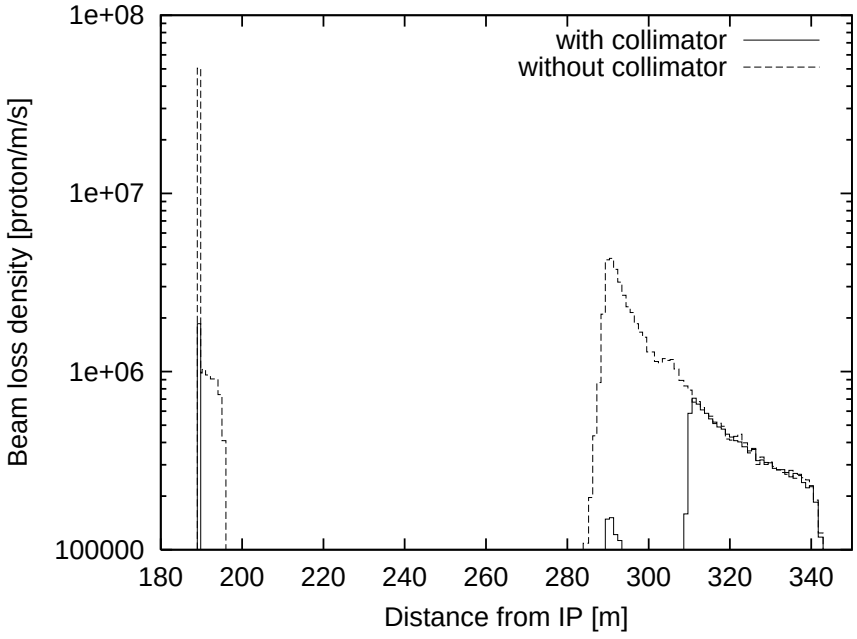

Figure 2: The beam loss density in the straight section and in the dispersion suppressor at the nominal luminosity $\mathcal{L}_o = 10^{34}$ cm^{-2}s^{-1}. The dashed histogram - without any collimators in the straight section. Solid histogram - the density with the collimator in operation. The integral of the losses in the dispersion suppressor (beyond the value of the abscissa 280 m)is $\dot{n} = 1.7\ 10^7$p/s with with collimator and $\dot{n} = 6.6\ 10^7$p/s without collimator.

and in Q5 is going on.

With this additional collimator, the beam loss density in the dispersion suppressor is well below the quench level even at the peak which is located in the dipole B9A ($\sim$310 m downstream of IP).

In Table 1, the peak density is correlated to the depth x_c at which the collimator jaw is set. The correlation indicates that some operational margin of the collimator can be used.

The momentum distribution of protons impacting on the collimator is wide and almost flat (see the dashed histogram in Figure 3). The transverse distribution is essentially associated to the dispersion at the collimation. The distribution $d^2N/d\delta_p d\Delta x_c$ with $\Delta x_c = |x - x_c|$ the impact parameter must therefore exhibit a strong correlation, which is in fact seen in our simulation (Figure 4). The following simple parametrisation of impact parameter and momentum distribution will therefore be used in the cascade calculations

$$\frac{x_c}{D_x^c} \leq \delta_p \leq 0.25, \tag{7}$$

$$\Delta x_c = D_x^c \delta_p - x_c, \tag{8}$$

$$\theta_x\ [mrad] \ = \ |x'| \ = \ 0.04 \ + \ 0.017 \Delta x_c, \tag{9}$$

with $D_x^c = 130$ mm the horizontal dispersion at the collimator location.

Table 1: Beam loss at the collimator and the peak loss density in the dispersion suppressor as functions of the collimator position x_c at the nominal luminosity 10^{34} cm^{-2}s^{-1}.

x_c [σ_x]	Loss at collimator [s^{-1}]	Peak loss density in DS [m^{-1}s^{-1}]
10	$9.3 \cdot 10^7$	$4.4 \cdot 10^5$
15	$8.8 \cdot 10^7$	$7.5 \cdot 10^5$
20	$8.3 \cdot 10^7$	$1.2 \cdot 10^6$

4.1 Quench in the Q5 of LHCb

It should be noted that the LHCb experiment will probably run at a luminosity of 2×10^{32} cm^{-2}s^{-1} which is a factor of 50 below the luminosity considered here. Thus, if one can simply scale the present results, the beam losses in Q5 should be a factor of ten below the quench limit. However if LHCb should require higher luminosities then a protection collimator could be needed especially since due to differences in the machine lattice between Points 1 and 5 and Point 8, simple scaling of the present results may not be adequate.

5 Beam losses in dispersion suppressor and arc

5.1 Cryogenic consideration

The rates of losses per element, normalised to the nominal luminosity are presented in Table 2, together with the corresponding power dissipation. These powers must be added to the existing load to be accomodated by the cryogenic system. They do not contain the beam-gas contribution to the beam losses. The integrated additional power between Q7 and Q13 is $\approx$ 20 Watts with the collimator at Q5 in operation. Without this collimator, the same integrated additional power would be $\approx$ 74 Watts. A former estimate of this load, deduced from [1] and integrated in overall cryogenic load review [9] was 10 Watts, a value which shall therefore be updated to $\approx$ 20 Watts.

5.2 Beam losses in dispersion suppressor and arc

Even with the collimator discussed in Section 4 in operation, the beam losses in the dispersion suppressor and in the adjacent arc cells remain the dominant factor for induced radioactivity and radiation damage. In the sequel, in Figures 5 and 6 and in Table 3, the rates, initially normalised to the nominal luminosity $\mathcal{L}_o$ are multiplied by a coefficient $\mathcal{L}_{eff}/\mathcal{L}_o = 0.5$ and correspond to an inelastic rate $\dot{n}_{inel} = 3.5 \cdot 10^8$ s^{-1} at the IP, according to [10].

The momentum losses could be compared with the loss density of $1.05 \cdot 10^4$ protons per metre per second which results from the beam-gas inelastic interactions which are expected in the early periods of operation.

Table 2: Integrated beam losses per elements of the dispersion suppressor, normalised to the nominal luminosity $\mathcal{L} = 10^{34}$ cm^{-2}s^{-1}, considering only the diffractive processes discussed in the text and with the collimator located near Q5 being active.

Element	Rate [proton/s]	Power [Watt]
B8A	$4.21 \cdot 10^4$	0.05
B8B	$1.19 \cdot 10^6$	1.33
QD8	$2.56 \cdot 10^5$	0.29
B9A	$7.22 \cdot 10^6$	8.09
B9B	$4.94 \cdot 10^6$	5.53
QF9A	$5.82 \cdot 10^5$	0.65
QF9B	$6.76 \cdot 10^4$	0.08
B11B	$1.52 \cdot 10^5$	0.17
drift	$2.03 \cdot 10^6$	2.27
QT.QF11	$1.34 \cdot 10^5$	0.15
QF11	$1.29 \cdot 10^5$	0.14
MB	$2.32 \cdot 10^5$	0.26
drift	$1.76 \cdot 10^5$	0.20
QT.QF13	$3.81 \cdot 10^4$	0.04
QF13	$1.26 \cdot 10^5$	0.14
Total	$1.73 \cdot 10^7$	19.38

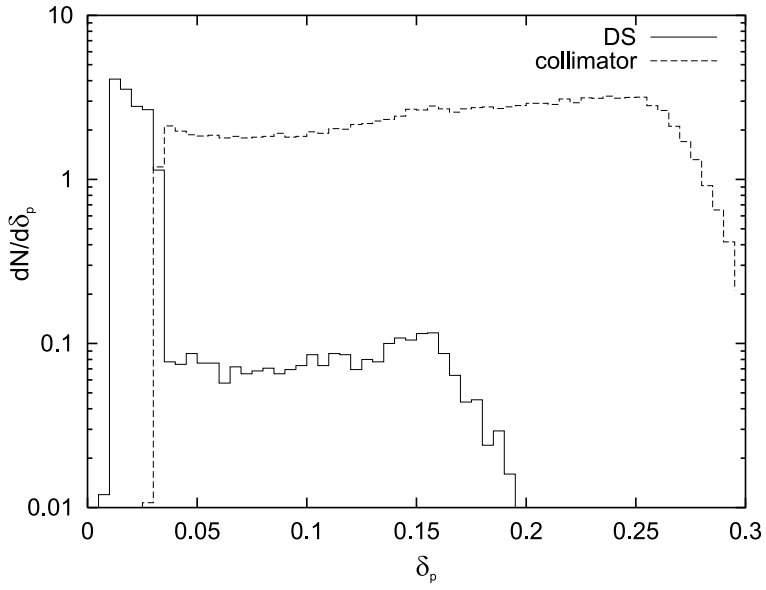

Figure 3: The momentum distributions of the lost protons. Dashed histogram - the protons intercepted by the collimator, solid one - those one lost in the dispersion suppressor and in the arc cells, including the protons which are reemitted by the collimator.

A general view of the beam loss distribution is presented in Figure 5. The beginning of the dispersion suppressor is located at 268.9 m from the IP and the arc starts at 437 m from the IP. The most impressive first group of losses corresponds to the region B8-Q9. It is shown in more details in Figure 6. The second group in Figure 5 marks the end of the DS. More downstream, the three narrow peaks are the losses in the arc cells. They are concentrated near the entrances of the focusing quadrupoles QF13, QF15 and QF17 respectively. We can expect similar but weaker losses near QF19 and beyond, but their density will not exceed the beam-gas loss density. The detailed longitudinal distribution of the beam losses is presented in Table 3 for further radiological assessments.

The angular distribution of the lost protons is shown in Figure 7 where x' is the angle of proton incidence on the beam screen. Three groups can be distinguished in the angle distribution. The first one with $x' \leq 0.4$ mrad corresponds to the losses downstream of QF9 i.e. in the tail of DS and in the arc cells. The second group with 0.5 mrad$\leq x' \leq 1$ mrad corresponds to B9A,B and QF9 and the third one with 1 mrad$\leq x' \leq 2.1$ mrad - to B8B and QD8.

6 Dose to machine components

The annual dose to components in the LHC ring is based on a 24-hour average luminosity which is a factor of two lower than the $10^{34}\,\mathrm{cm}^{-2}\mathrm{s}^{-1}$ considered in the previous sections [9]. Figure 5 shows the beam losses in B8 and the downstream elements scaled to this luminosity. Annual doses to components in the arcs have been calculated using a beam loss of 1.05×10^4 protons per metre [11]. From Figure 5 it will be seen that the maximum loss

Table 3: Beam loss density $\dot{n}$ in the elements of the dispersion suppressor and in the elements of the adjacent arc cells. The losses correspond to $3.5 \cdot 10^8$ inelastic interactions per second in the IP. s_{entr} is the distance between the IP and the element entrance. l_{elem} is the length of the element.

Name	s_{entr} [m]	l_{elem} [m]	$\dot{n}$ [p/m/s]	Name	s_{entr} [m]	l_{elem} [m]	$\dot{n}$ [p/m/s]
B8A	278.78	1.021	1798	B9A	312.73	1.021	304951
B8A	279.80	1.021	1648	B9A	313.76	1.021	291464
B8A	280.82	1.021	2772	B9A	314.78	1.021	271234
B8A	281.84	1.021	2997	B9A	315.80	1.021	255499
B8A	282.86	1.021	5919	B9A	316.82	1.021	244260
drift	283.88	1.360	7200	B9A	317.84	1.021	237517
B8B	285.24	1.021	8841	B9A	318.86	1.021	222531
B8B	286.27	1.021	17982	B9A	319.88	1.021	214289
B8B	287.29	1.021	24500	B9A	320.90	1.021	204549
B8B	288.31	1.021	45929	B9A	321.93	1.021	201552
B8B	289.33	1.021	74177	drift	322.95	1.360	189000
B8B	290.35	1.021	75675	B9B	324.31	1.021	179074
B8B	291.37	1.021	60765	B9B	325.33	1.021	182820
B8B	292.39	1.021	56344	B9B	326.35	1.021	158095
B8B	293.42	1.021	45780	B9B	327.37	1.021	159593
B8B	294.44	1.021	41509	B9B	328.39	1.021	154348
B8B	295.46	1.021	40760	B9B	329.42	1.021	153599
B8B	296.48	1.021	30794	B9B	330.44	1.021	143109
B8B	297.50	1.021	27572	B9B	331.46	1.021	140861
B8B	298.52	1.021	24426	B9B	332.48	1.021	140861
drift	299.54	1.910	22669	B9B	333.50	1.021	135617
QD8	301.45	.960	19204	B9B	334.52	1.021	128124
QD8	302.41	.960	17850	B9B	335.54	1.021	134118
QD8	303.37	.960	18168	B9B	336.57	1.021	132619
QD8	304.33	.960	16893	B9B	337.59	1.021	119133
QD8	305.29	.960	16256	drift	338.61	.955	111345
drift	306.25	1.198	16347	drift	339.56	.955	114549
drift	307.45	1.198	14367	QF9A	340.52	1.200	92437
B9A	308.65	1.021	79422	QF9A	341.72	1.200	58777
B9A	309.67	1.021	291464	drift	342.92	.400	36911
B9A	310.69	1.021	354402	QF9B	343.32	.850	22410
B9A	311.71	1.021	328178				

Table 3 continued

Name	s_{entr} [m]	l_{elem} [m]	$\dot{n}$ [p/m/s]	Name	s_{entr} [m]	l_{elem} [m]	$\dot{n}$ [p/m/s]
B11B	414.05	1.021	3296	MB	534.92	1.021	5394
B11B	415.07	1.021	10190	MB	535.94	1.021	9815
B11B	416.09	1.021	19181	MB	536.96	1.021	20754
B11B	417.11	1.021	41659	MB	537.98	1.021	32817
drift	418.14	1.062	54961	MB	539.00	1.021	42558
drift	419.20	1.062	62525	drift	540.02	1.740	50560
drift	420.26	1.062	73474	QT	541.76	.320	59526
drift	421.32	1.062	69008	drift	542.08	.305	57688
drift	422.38	1.062	69368	QF13	542.39	.775	42840
drift	423.45	1.062	70088	QF13	543.16	.775	15892
drift	424.51	1.062	62597	MB	642.84	1.021	3221
drift	425.57	1.062	66703	MB	643.86	1.021	10714
drift	426.63	1.062	66991	MB	644.88	1.021	18132
drift	427.69	1.062	60796	MB	645.90	1.021	26823
drift	428.76	1.062	62885	drift	646.92	1.740	42382
drift	429.82	1.062	59788	QTF	648.66	.320	47812
drift	430.88	1.062	60364	drift	648.98	.305	59444
drift	431.94	1.062	59644	MB	750.76	1.021	1273
drift	433.00	1.062	57338	MB	751.78	1.021	4195
QT	434.07	1.150	58273	MB	752.80	1.021	8541
drift	435.22	.275	61200	drift	753.82	1.740	18993
QF11	435.49	.775	45307	QTF	755.56	.320	24623
QF11	436.27	.775	15990	drift	755.88	.305	32857
MB	533.90	1.021	1498	QF17	756.18	.775	24282

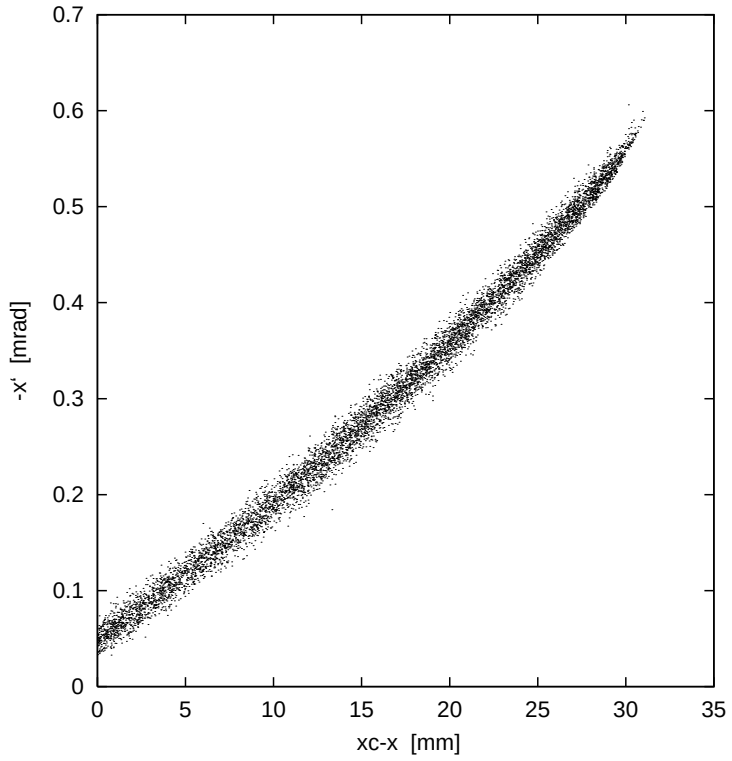

Figure 4: The scatter plot of the proton incidence on the collimator. x_c is the horizontal position of the collimator jaw, $x_c - x$ the impact parameter and$x' = dx/ds$.

in B8 with the protection collimators in place is 3.5×10^5 protons per metre, with losses in the other downstream magnets close to 5×10^4 protons per metre. To a first approximation, one can simply scale the doses in the arcs to the new loss rates in order to obtain the annual doses in the dispersion suppressor regions close to the high-luminosity experiments. These doses could then be a factor of 30 higher than the arc doses around B9, even higher near Q5 and a factor of 5 higher than the arc doses close to the other magnets.

Care in the selection of components must also be taken in the dispersion suppressor region of Point 8 since even though the luminosity will be lower, a protection collimator may not be installed. In this case the annual doses in the region of B8 of this dispersion suppressor could be a factor of 8 higher than the arc doses with higher doses around Q5.

More accurate estimates of the doses due to these beam losses will require significant time and effort to be spent on cascade simulations.

7 Conclusions

A more careful review of diffractive and other closely related processes in proton-proton collisions revealed that the losses of protons in the dispersion suppressors of the experimental areas will be larger than previously foreseen. A collimator must be installed in the downstream beam channels of IP1 and IP5 near the quadrupole Q5, both to prevent a quench at

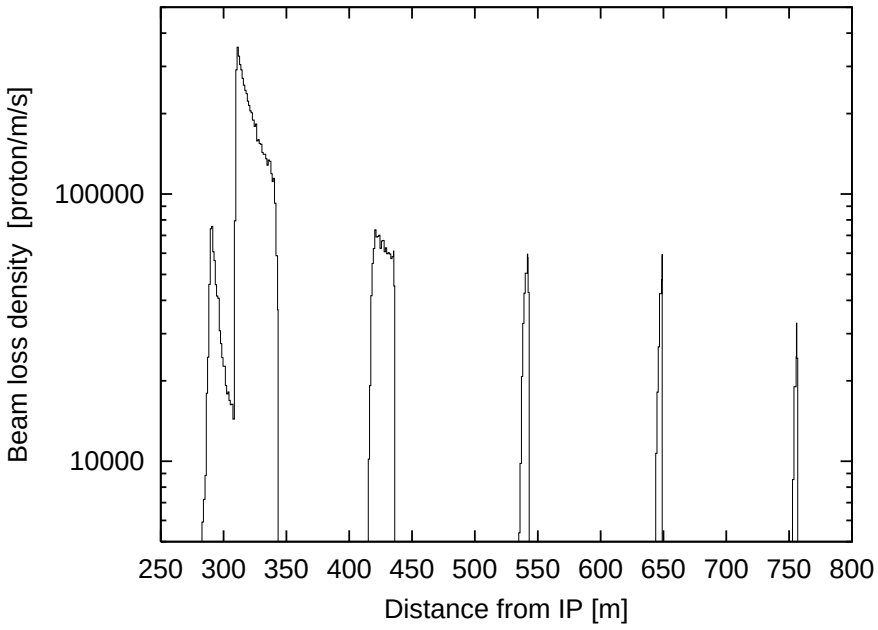

Figure 5: Beam loss density in the dispersion suppressor and in the adjacent arc cells at the average luminosity. The corresponding inelastic interaction rate in the IP is $3.5 \cdot 10^8$ s^{-1} [10].

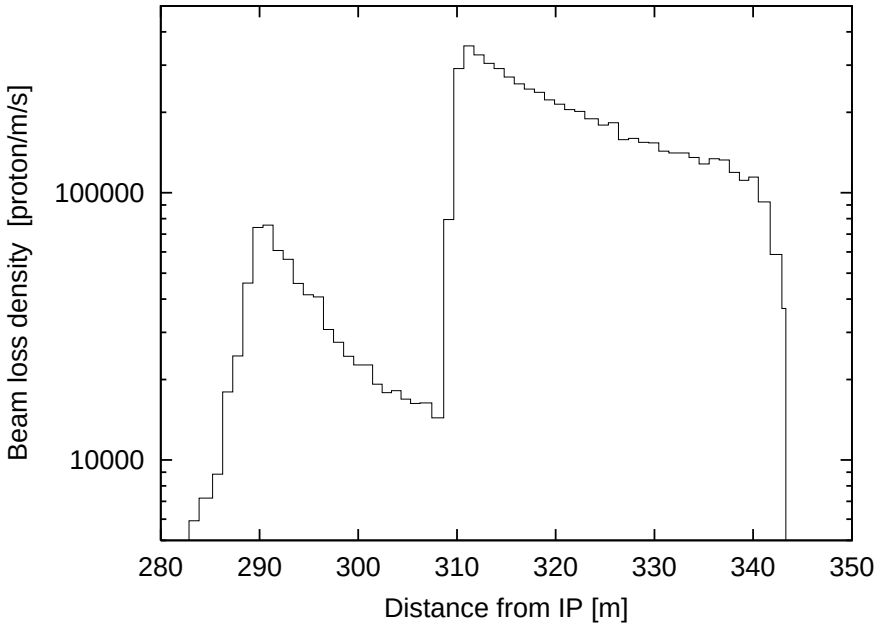

Figure 6: The same as Figure 5 for B8-QF9 region.

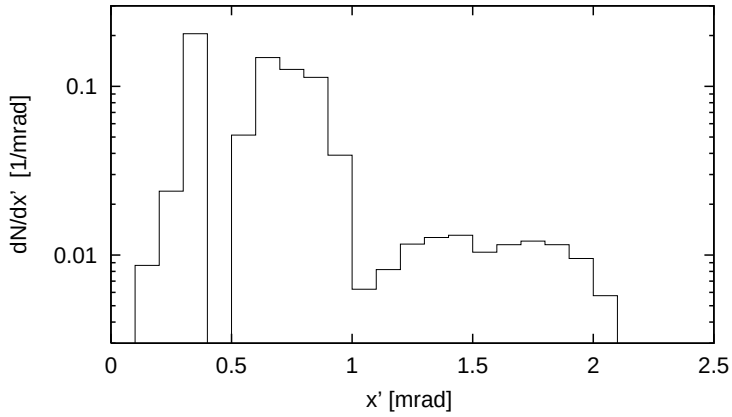

Figure 7: The angular distribution of the protons lost in the dispersion suppressor and in the arc cells.

Q5 and a risk of quench near the bending magnets B8. These collimators shall also reduce the cryogenic load at 1.9K from 78 Watts down to 20 Watts. A further check of the impact of such processes in IP2 and IP8 will be made. An impact study of the absorption of protons in the collimator near Q5 by nuclear cascade is going on. The present work will serve as an input for radiological studies in the dispersion suppressors of the experimental insertions. As already said in the introduction, a more detailed work is going on, taking into account recently foreseen changes. A definitive proposal will be formulated in a further document.

Acknowledgements

We had the benefit of the advice of J.P. Koutchouk and the help of W. Herr for the use of new optics and the definitions of the crossing bumps.

References

[1] J.B. Jeanneret, LHC Project Note 211, October 1992.

[2] Field R.D., Fox G.S., Nucl.Phys.B, 1974, v.80, p.367.

[3] Barashenkov V.S., Slavin N.V., Acta Phys.Polon.B, 1981, v.10, p.563-573.

[4] I.Baishev, A.Drozhdin and N.Mokhov, SSCL-MAN-0034, Dallas, March 1994.

[5] J.B.Jeanneret and R.Ostojic, LHC Project Note 111, September 1997.

[6] N.Catalan Lasheras et al., CERN LHC Report 156, 1997.

[7] J.B.Jeanneret et al,CERN LHC project report 44,1996.

[8] I.Baishev, Preprint IHEP 87-147, Serpukhov, 1987.

[9] L.Tavian and U.Wagner, LHC Project Note 140, 1997.

[10] M. Hofert, K.Potter and G.R. Stevenson, CERN/TIS-RP/IR/95-19.1, July 1995.

[11] LHC Engineering Specification, *General parameters for equipment installed in the LHC*, LHC Project Document No. LHC-PM-ES-0002.00 (1999)